Dyes and Pigments 201 (2022) 110227

Contents lists available at ScienceDirect

Dyes and Pigments

journal homepage: www.elsevier.com/locate/dyepig

A mitochondria-tracing fluorescent probe for real-time detection of mitochondrial dynamics and hypochlorous acid in live cells

Nansong Zhu [a], Xiaolei Guo [a], Yulei Chang [c], Zhan Shi [a,*], Long Yi Jin [b,**], Shouhua Feng [a]

[a] State Key Laboratory of Inorganic Synthesis and Preparative Chemistry, College of Chemistry, Jilin University, Changchun, 130012, PR China
[b] Department of Chemistry, National Demonstration Centre for Experimental, Chemistry Education, Yanbian University, Yanji, 133002, PR China
[c] State Key Laboratory of Luminescence and Applications, Changchun Institute of Optics, Fine Mechanics and Physics, Chinese Academy of Sciences, Changchun, 130033, China

ARTICLE INFO

Keywords:
Hypochlorous acid
Fluorescent probe
Mitochondria-tracing
Live cells
Biological imaging
Synthetic method

ABSTRACT

Mitochondrial dynamics and hypochlorous acid (HOCl) are involved in many physiological and pathological processes. Therefore, the development of real-time analysis tools for biological studies involving mitochondrial dynamics and HOCl is highly significant. Herein, we report a fluorescent probe, **RIC**, consisting of rhodamine, imidazolium salt, and coumarin, which has high selectivity and sensitivity toward HOCl. **RIC** has an inherently blue fluorescence signal and can be anchored in mitochondria, which enables it to reveal changes in mitochondrial dynamics. This mitochondria-anchoring characteristic also facilitates the real-time detection of HOCl in mitochondria. To our knowledge, **RIC** is the first probe to detect mitochondrial dynamics and HOCl in real time. The detection limit of HOCl is as low as 3.8 nM, and **RIC** analyzes endogenous and exogenous HOCl in live cells. The detection capacity is pH-insensitive in the physiological pH range of mitochondria, and the HOCl-sensing process is completed within seconds in cuvettes. Furthermore, we prove that the molecular design strategy provides a general synthetic method for constructing new multifunctional probes for HOCl.

1. Introduction

Hypochlorous acid (HOCl), an important reactive oxygen species (ROS), is involved in many cellular processes. Abnormal HOCl levels generated by myeloperoxidase and dual oxidase cause many diseases, including kidney disease, metabolic syndrome, atherosclerosis, pulmonary inflammation, rheumatoid arthritis, cardiovascular disease, skin inflammation, neuronal disease, and cancer [1–3]. Therefore, the sensing of HOCl levels in physiology and pathology is crucial. As a mature and progressive technology, fluorescence imaging has super temporal and spatial resolution and allows real-time analysis in biological environments. To provide analysis tools for the early detection of HOCl-related diseases and further explore the critical roles of HOCl in cellular signaling pathways, numerous fluorescent probes targeting HOCl have been synthesized and applied to cells, tissues, zebrafish, and mice [4–33].

Recently, the significance of fluorescent probes for detecting mitochondrial HOCl levels has been demonstrated in physiology and pathology [34–45]. Most of the existing probes in this respect are cationic dyes and accumulate in the negative mitochondrial matrix, which is a result of plasma and mitochondrial membrane potentials (MMPs). Once MMP declines (i.e., mitochondria are depolarized), they may leak out of mitochondria to some extent. This leads to a decreased probe concentration and varied probe localization, which are roadblocks to real-time detect mitochondrial HOCl, thus, limiting practical applications.

To solve the problem of dye leakage from mitochondria, a few methods have been proposed to construct mitochondria-immobilized or -anchoring probes [46–55]. As the word suggests, probes with the concept "mitochondria-anchoring" can be retained in depolarized mitochondria, which guarantees the relatively constant concentration and localization of the probes and can help to trace mitochondria by the inherently robust fluorescence signal. Recently, our research group reported a mitochondria-anchoring probe, **ZED**, for the simultaneous detection of thiols, HOCl, and mitochondrial status in cancer cells [56]. **ZED** reacted with thiols to transform into **ZED-1** (Scheme 1) in live cells, and **ZED-1** was anchored in the mitochondria. Compared with other mitochondria-immobilized probes, there is no known fixed group in the structure of **ZED-1**, and **ZED-1** is probably anchored via interactions

* Corresponding author.
** Corresponding author.
E-mail addresses: zshi@mail.jlu.edu.cn (Z. Shi), lyjin@ybu.edu.cn (L.Y. Jin).

https://doi.org/10.1016/j.dyepig.2022.110227
Received 21 January 2022; Received in revised form 3 March 2022; Accepted 4 March 2022
Available online 12 March 2022

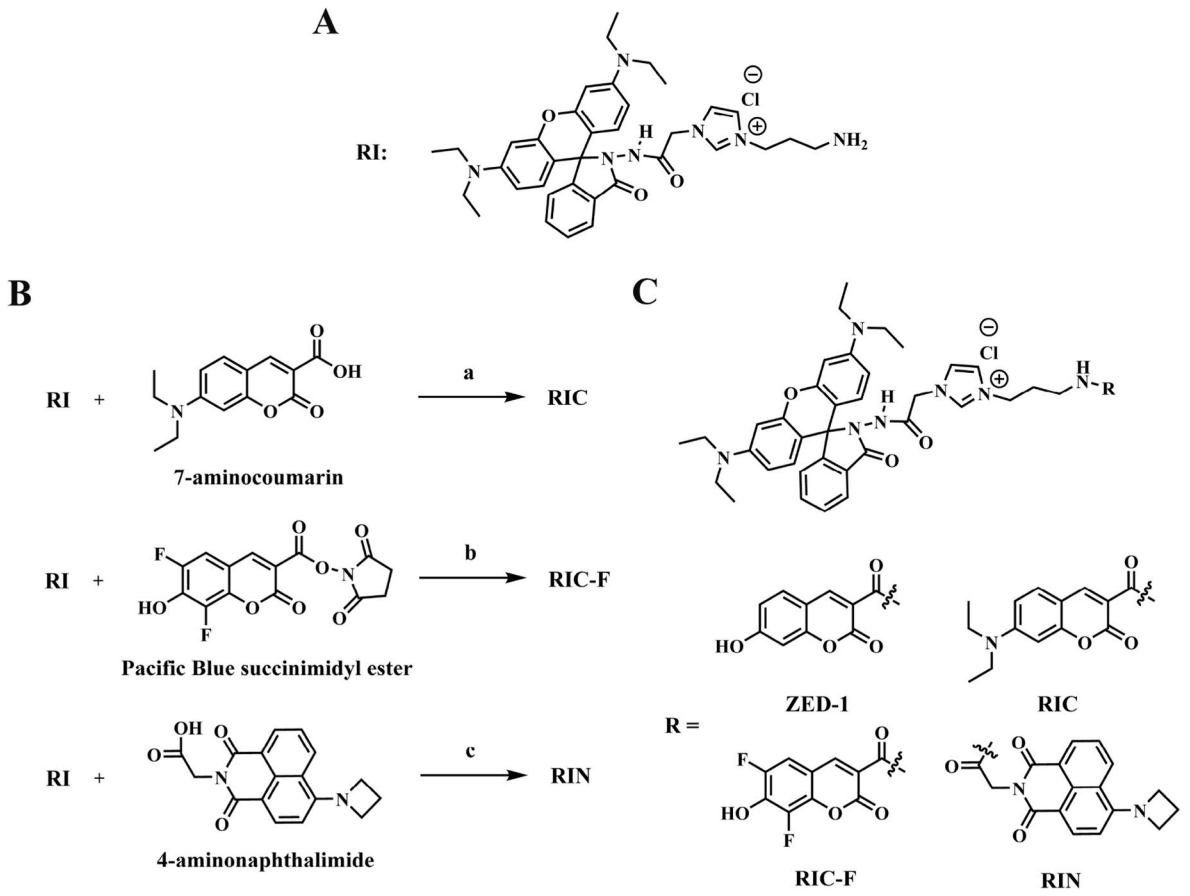

Scheme 1. The synthetic routes and molecular structures of compounds. (A) The molecular structure of **RI**. (B) The synthetic routes of **RIC**, **RIC-F**, and **RIN**. Conditions: (a) R.T., EDCI, TEA, DMAP. (b) 100 °C, TEA. (c) R.T., HATU, DIEA. (C) The molecular structures of **ZED-1**, **RIC**, **RIC-F**, and **RIN**.

with the hydrophobic lipid bilayer in mitochondrial inner membrane [53], given that **ZED-1** has an organic molecular chain of atoms between the rhodamine and coumarin. Meanwhile, the positively charged imidazolium salt group may also interact with cardiolipin (an abundant and negatively charged component of the lipid bilayer) in mitochondrial inner membrane through electrostatic interactions [57]. **ZED-1** has an inherently blue fluorescence signal (I_{450}) that traces polarized mitochondria. However, I_{450} was sensitive to mitochondrial pH (MpH) fluctuations (normally 7–8) [58] and could not provide a sufficient signal-to-background ratio when MpH decreased along with the decline in MMP. Accordingly, **ZED** could barely trace depolarized mitochondria in the absence of permeability transition pore openings.

Common mitochondrial dynamics (mitochondrial fission and fusion) are associated with many aspects of mitochondrial function, and a variety of diseases are related to disturbed mitochondrial dynamics [59]. In addition to detecting HOCl, the inherently robust mitochondria-tracing fluorescence signals from mitochondria-anchoring HOCl probes can monitor mitochondrial dynamics by revealing changes in mitochondrial morphology [60], reflecting alterations in mitochondrial functions and disease states. Similar to their ability to detect mitochondrial morphology, mitochondria-tracing HOCl probes have the potential to detect other mitochondrial dynamics, such as mitochondrial movements within a cell [61], interactions with other organelles [62], and autophagy [63,64], confirming the high significance of studying these probes. However, no studies have demonstrated the syntheses and applications of such unimolecular probes that trace both polarized and depolarized mitochondria, and no analytical method involving multiple probes that can achieve the same functions has been reported so far.

To the best of our knowledge, **ZED-1** is one of the few mitochondria-anchoring HOCl probes with an inherent fluorescence signal. Considering difficulties in molecular design and preparation, it is much easier to obtain new mitochondria-tracing HOCl probes by modifying a known structure than by designing a new one. Although there has been another report on the HOCl probe that can be retained in depolarized mitochondria [65], the mitochondria-tracing capacity of this molecule still needs to be carefully investigated. Therefore, in order to solve the urgent problem of a current lack of such probes, we altered the structure of **ZED-1** to obtain another mitochondria-anchoring HOCl probe (**RIC**, Scheme 1). The blue fluorescence signal of **RIC** is free from MpH fluctuations and is, thus, unlike **ZED**, capable of tracing both polarized and depolarized mitochondria. **RIC** can also reveal dynamic changes in mitochondrial morphology, confirming the mitochondria-tracing capacity.

Apart from the mitochondria-tracing capacity, **RIC** has great sensitivity (detection limit = 3.8 nM) and selectivity toward HOCl. In addition, **RIC** analyzes endogenous and exogenous HOCl with excellent detection capacities in live cells. Furthermore, we demonstrate the universality of this "alteration" design strategy from the additional successful syntheses of **RIN** and **RIC-F** (Scheme 1), which presents a general synthetic method for obtaining new multifunctional probes for HOCl.

2. Materials and methods

2.1. General information

Unless otherwise noted, all solvents and reagents used in this study were of reagent grade, purchased from commercial suppliers, and used without further purification. Water was twice distilled in all experiments before use. Bruker instruments were employed to record ^{1}H NMR (400

MHz), ^{13}C NMR (100 MHz), and LC-HRMS (high-resolution mass spectra combined with liquid chromatography). An Edinburgh FLS920 spectrofluorometer equipped with both continuous (450 W) and pulsed xenon lamps was used to analyze the fluorescence samples. Fluorescence imaging of live cells was performed using a confocal laser scanning microscope (Nikon, Japan). A BioTek microplate reader was used for cytotoxicity assays. Thin silica gel plates and silica gel (mesh 200–300) were used for TLC analysis and flash column chromatography, respectively.

2.2. The syntheses and characterizations of *RIC, RIN, and RIC-F*

The synthetic routes of **RIC**, **RIN**, and **RIC-F** are shown in Scheme 1.

2.2.1. The synthesis and characterization of *RIC*

7-(Diethylamino)-2-oxo-2*H*-1-benzopyran-3-carboxylic acid (7-aminocoumarin, 13 mg, 0.05 mmol) was placed in a round-bottomed flask and 2 mL of DMF was then added. The mixture was sonicated for a few minutes to dissolve the 7-aminocoumarin. 3-(3-Aminopropyl)-1-(2-((3′,6′-bis(diethylamino)-3-oxospiro[isoindoline-1,9′-xanthen]-2-yl) amino)-2-oxoethyl)-1*H*-imidazole-3-ium chloride (rhodamine-imidazolium salt, **RI**, 33 mg, 0.05 mmol) was added and the mixture was stirred. To the stirred solution, 1-(3-dimethylaminopropyl)-3-ethylcarbodiimide hydrochloride (EDCI, 11.5 mg, 0.06 mmol) was added, following the addition of 4-dimethylaminopyridine (DMAP, 0.6 mg, 0.005 mmol) and triethylamine (TEA, 21 μL, 0.15 mmol). The mixture was allowed to react overnight at room temperature, and this was monitored by TLC to confirm completion. Next, the DMF solution was washed with water and extracted with CH_2Cl_2. The organic phase was then dried using anhydrous Na_2SO_4 and concentrated under a vacuum. The residue was redissolved in CH_2Cl_2 and purified by flash column chromatography with eluents of CH_2Cl_2 and CH_3OH to obtain **RIC** (34.2 mg, 76% yield) as a red solid. ^{1}H NMR (DMSO-d_6, 400 MHz) δ [ppm]: 10.24 (s, 1H), 9.11 (s, 1H), 8.72 (t, J = 6.0 Hz, 1H), 8.65 (s, 1H), 7.83 (dd, J = 9.1 Hz, 1H), 7.79 (t, J = 1.8 Hz, 1H), 7.68 (d, J = 6.8 Hz, 1H), 7.61–7.51 (m, 2H), 7.39 (t, J = 1.8 Hz, 1H), 7.04 (d, J = 6.8 Hz, 1H), 6.81 (dd, J = 9.1, 2.4 Hz, 1H), 6.62 (d, J = 2.4 Hz, 1H), 6.52 (s, 1H), 6.50 (s, 1H), 6.35 (d, J = 2.6 Hz, 2H), 6.32 (d, J = 2.6 Hz, 2H), 4.99 (s, 2H), 4.26–4.19 (m, 2H), 3.49 (q, J = 6.9 Hz, 4H), 3.37–3.23 (m, 8H), 2.04 (t, J = 6.8 Hz, 2H), 1.14 (t, J = 7.0 Hz, 6H), 1.08 (t, J = 6.9 Hz, 12H). ^{13}C NMR (DMSO-d_6, 100 MHz) δ [ppm]: 164.59, 164.44, 164.02, 162.49, 161.32, 156.72, 153.44, 152.34, 148.91, 148.51, 137.83, 134.01, 132.34, 129.54, 129.04, 128.34, 124.36, 123.80, 123.20, 122.46, 114.95, 113.99, 111.41, 108.19, 104.37, 102.32, 97.54, 65.57, 49.71, 47.45, 44.11, 36.43, 30.19, 12.92. LC-HRMS (m/z): Found for $C_{50}H_{57}N_8O_6^+$ ([M]$^+$): 865.4424; Calcd.: 865.4396.

2.2.2. The syntheses and characterizations of *RIN and RIC-F*

Details of the syntheses and characterizations of **RIN** and **RIC-F** are presented in the Supporting Information.

2.3. Fluorescence measurements in cuvettes

Concentrated solutions of ROS, ions, and GSH were prepared according to the methods of previous studies [66–69]. Dry DMSO was used to prepare stock solutions of 5 mM of **RIC**, **RIN**, and **RIC-F**. Freshly prepared solutions were stored at −20 °C and used within 1 week. Before adding concentrated solutions of analytes, the stock solutions were directly diluted with 1000 times PBS buffer (50 mM) and then allowed to stand for an appropriate time at room temperature. The fluorescence spectra of the solutions were measured in 1 cm quartz cells.

2.4. Cytotoxicity assays

Cells were cultured in high-glucose Dulbecco's modified Eagle's medium (DMEM) without phenol red, supplemented with 1 mM sodium pyruvate, 1 mM GlutaMAX™ (a dipeptide formed by alanine and glutamine), and 10% fetal bovine serum at 37 °C under an atmosphere of 95% air and 5% CO_2. Cells were then inoculated into 96-well plates at a density of 1 × 10^5/well and cultured overnight. After that, cells in the experimental groups were treated with complete medium (0.1% DMSO) containing 5, 10, and 15 μM **RIC** for 30 min. The control groups were treated with complete medium (0.1% DMSO) for 30 min. Cells were then washed three times with PBS (pH 7.4, 10 mM) and fresh medium was added. After growing for one night, cell counter kit 8 reagent was added to the wells and maintained for another 2 h. The absorbance at 450 nm was measured using a microplate reader. The optical densities (ODs) of the six wells in the control and experimental groups were tested, and the average value of each group was recorded as the OD control and OD experimental group, respectively. Cell viability was calculated using the following formula:

$$\text{Cell viability} = \text{OD experimental group/OD control group} \times 100\%$$

2.5. Confocal imaging in live cells

Cells were inoculated at suitable densities in glass-bottom dishes to ensure they reached exponential phase before the confocal experiments. After growing for the same amount of time in the dishes, the cells were treated with **ZED-1**, **RIC**, **RIN**, **RIC-F**, and other commercial reagents in complete medium for the indicated time. Before the reagents were added each time, the cells were washed carefully with PBS buffer (pH 7.4, 10 mM) three times, and fresh FluoroBrite™ DMEM was added to the dishes before pictures were captured in situ using a confocal laser scanning microscope. The relative pixel intensities of the pictures were then calculated using ImageJ software.

3. Results and discussion

To date, reports on the skeleton structures of mitochondria-anchoring probes, which have an inherent fluorescence signal, that are available to construct new mitochondria-tracing HOCl probes are rare. Therefore, we attempted to obtain these novel probes by changing the molecular structure of **ZED-1**, which has an inherently blue fluorescence I_{450} signal sensitive to MpH alterations and a turn-on red fluorescence produced by the reaction of rhodamine hydrazides with HOCl. To this end, we changed the MpH-sensitive molecule from 7-hydroxycoumarin to 7-aminocoumarin, 4-aminonaphthalimide, and Pacific Blue, considering their excellent sensing behaviors in biological environments in the literature [70–74]. Three fluorophores (**RIC**, **RIN**, and **RIC-F**) probably insensitive to MpH alterations due to the presence of MpH-insensitive amino groups and ortho-difluorinated hydroxyl group, which has a lower pK_a, were obtained (Scheme 1). The synthetic routes showed that the primary amine of **RI** could react with fatty acids, aromatic acids, and other succinimidyl esters to obtain products with moderate yields, demonstrating the good nucleophilic capability of the amine. In addition, all three new probes were capable of detecting HOCl in buffer solutions (Fig. S1), indicating that the HOCl receptor unit has a relatively universal recognition ability in the absence of other HOCl-sensitive groups. Thus, the successful syntheses of the compounds also show that this "alteration" design strategy provides a general synthetic method to construct new multifunctional HOCl probes through the combination of **RI** and other functional fluorophores that are tolerated in condensation reactions.

With these compounds in hand, we first tested the mitochondria-targeting capacity to screen out probes for further research. Although Mito-Tracker Red CMXRos (MTR, a commercial dye for mitochondrial morphology) has a non-negligible spectral overlap with the red fluorescence of the probes utilized to sense native HOCl in cancer cells, the red fluorescence of MTR was much brighter than that of the probes.

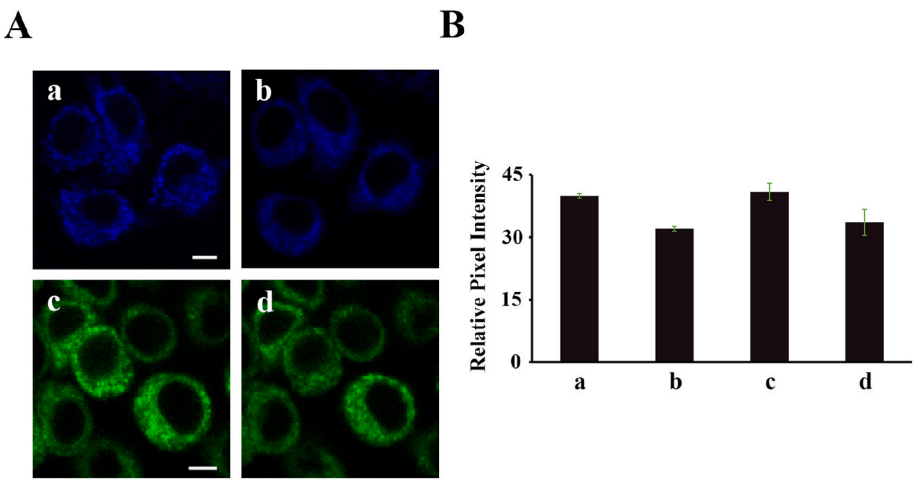

Fig. 1. Confocal experiments in RAW264.7 cells. (A) Images of the cells. (a) Cells incubated with 5 μM **RIC** for 30 min. (b) Cells from (a) further treated with 30 μM CCCP for 30 min. (c) Cells incubated with 1 μM MTG for 10 min. (d) Cells from (c) further treated with 30 μM CCCP for 30 min. (B) Relative pixel intensity of the related images in (A). The results are presented as mean ± standard deviation (n = 3). (a, b) and (c, d) were excited at 405 and 488 nm and collected within 417–477 and 499–529 nm, respectively. Scale bar: 5 μm.

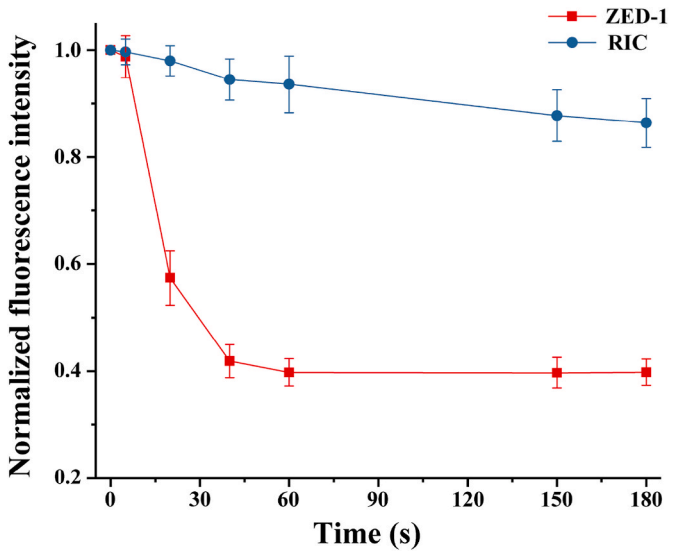

Fig. 2. The dynamic changes of fluorescence intensity in MCF-7 cells. Two separate groups of cells were incubated with 5 μM **ZED-1** and **RIC** for 30 min, respectively. And the cells were then treated with 30 μM CCCP for 180 s. The fluorescence was excited at 405 nm and collected within 417–477 nm. The results are presented as mean ± standard deviation (n = 3).

Therefore, MTR could be used for mitochondrial colocalization experiments involving the probes. As shown in Figs. S2 and S3, the blue (I_{480}) and green (I_{550}) inherent fluorescence from coumarin and naphthalimide of **RIC** and **RIN**, respectively, overlapped well with MTR in cytoplasm. Nevertheless, I_{550} was also retained in other punctate structures outside cytoplasm, which was probably caused by slower membrane permeability rates, enabling the accumulation of **RIN** in subcellular regions on the surfaces of the cells. In contrast, in addition to staining punctate regions, the blue fluorescence of **RIC-F** was retained in the edges of the cells (Fig. S4), indicating that **RIC-F** could not pass through the plasma membrane. Above all, we chose **RIC** as the probe discussed in this article for the real-time detection of mitochondrial dynamics and HOCl.

The cytotoxicity assays showed that **RIC** had little influence on cell viability up to 15 μM (Fig. S5), and we chose incubating cells with **RIC** for 30 min as the culture condition because of the sufficient accumulation of **RIC** in mitochondria. Before we aimed to check the ability of **RIC** to trace mitochondrial dynamics, the mitochondria-anchoring property was investigated. As shown in Fig. 1a and b, I_{480} remained at nearly 80% intensity after the cells were further treated with carbonyl cyanide 3-chlorophenylhydrazone (CCCP, a reagent that reduces both MpH and MMP) for 30 min, demonstrating that **RIC** was mitochondria-anchoring. Cells stained with Mito-Tracker Green FM (MTG, a commercial immobilized tracker for mitochondria) were used as the control group. When treating cells with CCCP under the same conditions, a similar loss of intensity was observed in MTG-stained cells (Fig. 1c and d), showing that **RIC** had a comparable mitochondria-anchoring capacity to MTG. Since MTG is also a probe that detects dynamic changes in mitochondrial mass [75], we deduced that this loss of intensity was probably caused by the decrease in mitochondrial mass during the CCCP treatments.

A comparative experiment with I_{450} was then carried out to test our design idea that **RIC** was insensitive to MpH alterations probably due to the presence of MpH-insensitive amino group. As illustrated in Fig. 2, I_{450} declined sharply upon the addition of CCCP, whereas I_{480} decreased gradually by a small amount. After the same CCCP treatment for 60 s, I_{450} declined to 40% intensity, but I_{480} remained at over 90% intensity. According to previous studies, lower dosages of CCCP can cause complete uncoupling of mitochondria and reduce MpH to the minimum within 60 s [76]. Therefore, the comparison of the fluorescence intensities within 60 s shows that **RIC** is insensitive to MpH alterations and proves the correctness of our design idea. The insensitivity ensures the brightness of **RIC** in live cells and guarantees that **RIC** can always offer a sufficient signal-to-background ratio during sensing applications. Besides, the gradual reduction in I_{480} after 60 s also demonstrates a dynamic decrease in mitochondrial mass.

Next, we utilized **RIC** to monitor the changes in mitochondrial morphology to verify the feasibility of our design strategy for constructing mitochondria-tracing HOCl probes. The mitochondria-targeting property of **RIC** was further confirmed by co-staining cells with MTR (Fig. 3a–c) and the Pearson's correlation coefficient was calculated as 0.90 (Fig. S6).The images also showed filamentous structures of normal mitochondria. When the cells were treated with 10 μM CCCP for 10 min to induce mitochondrial damage, some of the mitochondria changed into punctate structures (Fig. 3d–f), indicating changes in mitochondrial morphology caused by mitochondrial swelling in the presence of CCCP [77]. At the end of this mitochondrial process, I_{480} also overlapped with MTR (Pearson's correlation coefficient was 0.89; Fig. S7), showing that **RIC** real-time detected mitochondrial morphology similar to MTR. To confirm the mitochondria-tracing capacity of **RIC**, a high dosage of CCCP was used to induce greater mitochondrial damage. As shown in Fig. 3g–i, **RIC** presented fragmented mitochondria after the CCCP treatment, which was consistent with the fuzzy morphological structure demonstrated by the red fluorescence of MTR. As expected, **RIC** also had a good overlay with MTR when

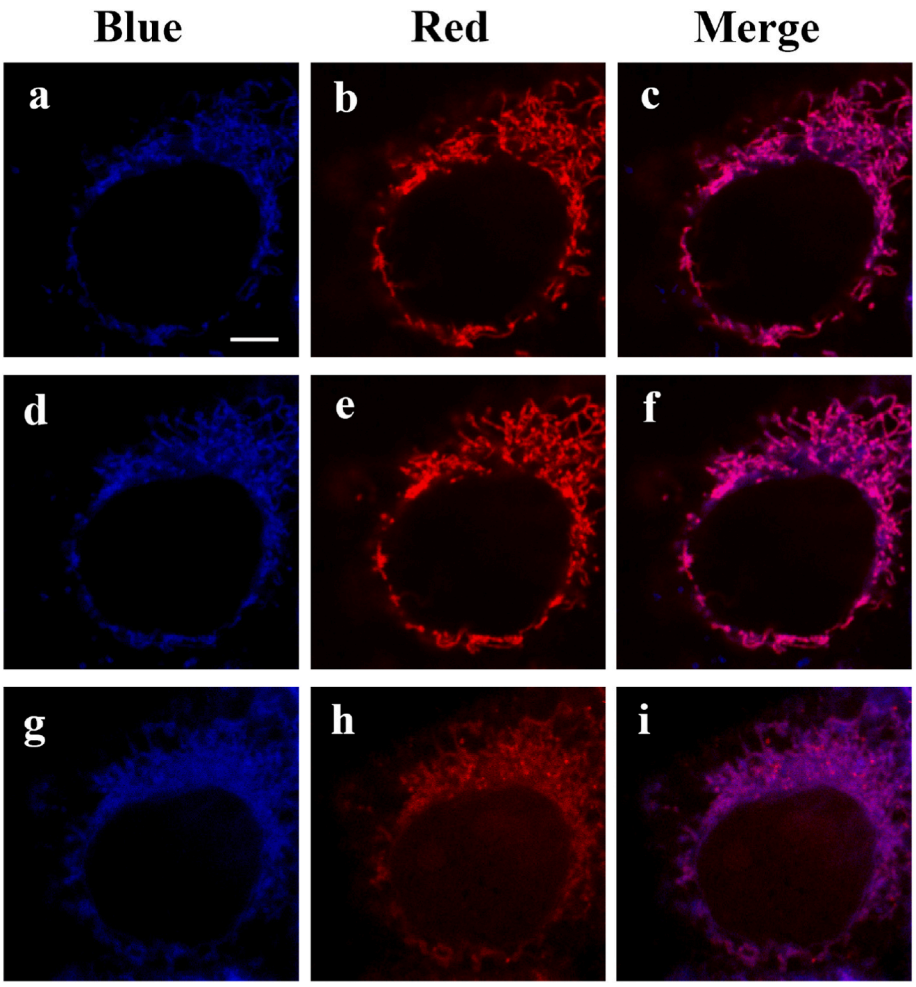

Fig. 3. Confocal experiments in MCF-7 cells. (a–c) Cells incubated with 5 μM **RIC** for 30 min and then treated with 200 nM MTR for 10 min (d–f) Cells from (a–c) further treated with 10 μM CCCP for 10 min (g–i) Cells from (d–f) further treated with 100 μM CCCP for 20 min. Blue and red channels were excited at 405 and 543 nm and collected within 417–477 and 553–618 nm, respectively. Scale bar: 5 μm. (For interpretation of the references to colour in this figure legend, the reader is referred to the Web version of this article.)

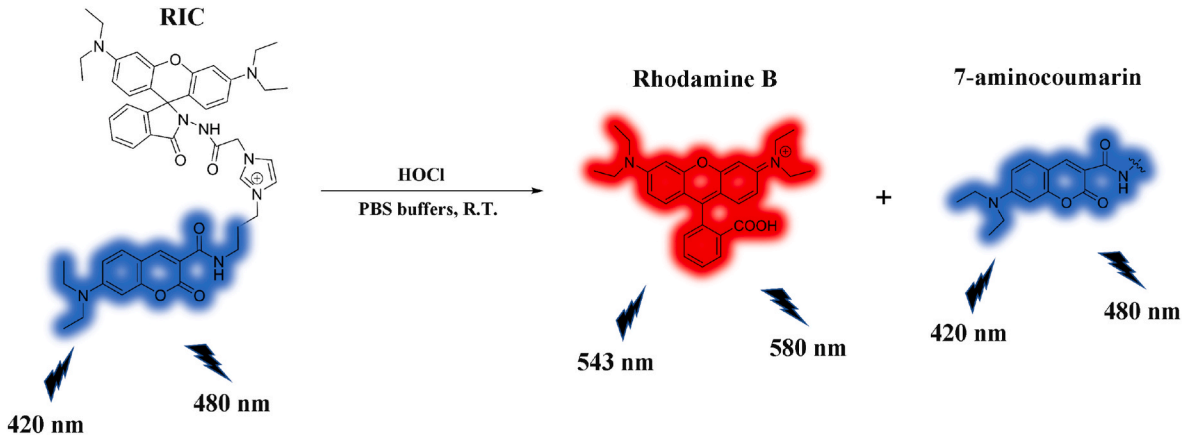

Fig. 4. The sensing mechanism of **RIC** toward HOCl in PBS buffers.

mitochondrial fragmentation occurred, and the Pearson's correlation coefficient was calculated as 0.82 (Fig. S8). These results suggest that **RIC** has a great mitochondria-tracing property comparable to MTR and can real-time detect mitochondrial dynamics.

Subsequently, we tested the HOCl-sensing properties of **RIC**. **RIC** has good water solubility due to the hydrophilic imidazolium salt; thus, we carried out fluorescence experiments in PBS buffers containing 0.1% DMSO. **RIC** detects HOCl via a known mechanism (Fig. 4) [49,56]. In brief, the hydrazides of **RIC** reacted with HOCl, generating a red fluorescence (I_{580}) from Rhodamine B (Fig. S9). I_{580} almost reached its maximum intensity within 5 s (Fig. 5A), showing a fast response of **RIC** in detecting HOCl. Since HOCl reacts with a large number of biological species in cells and, therefore, has a relatively short lifetime, this fast response is important for **RIC** to sense mitochondrial HOCl. In addition, the reactivity of **RIC** toward HOCl was not altered significantly in neutral and slightly alkaline solutions (Fig. 5B), indicating that the HOCl detection capacity of **RIC** is not susceptible to MpH fluctuations. The sensing performances of **RIC** toward HOCl decreased in acid solutions

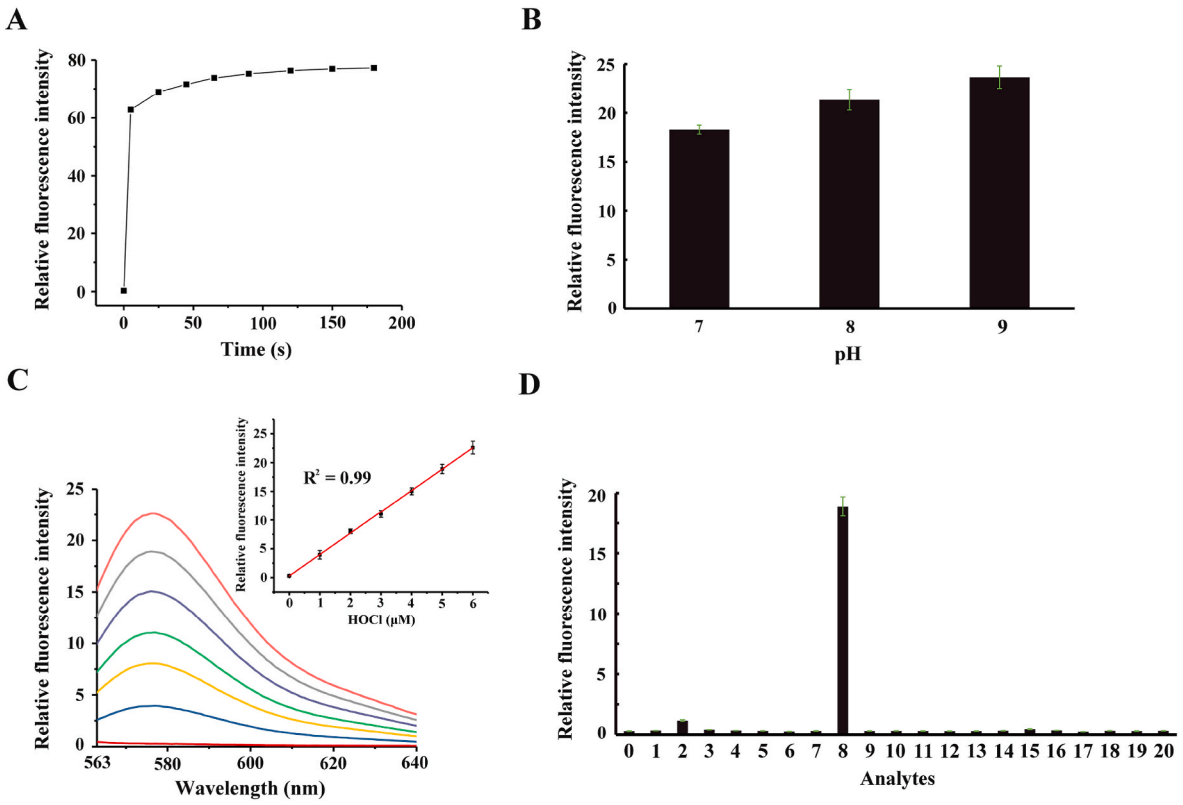

Fig. 5. The fluorescence experiments of 5 μM **RIC** in the presence of different analytes in PBS buffers (pH 8.0, 0.1% DMSO), excitation at 543 nm, slit width: 4/4 nm. (A) Time-dependent experiments involving 30 μM HOCl. (B) pH-dependent experiments involving 6 μM HOCl. (C) Fluorescence titration experiments involving 0–6 μM HOCl. (D) Different analytes, 0: blank; 1–7: 10 μM NO, $ONOO^-$, H_2O_2, O_2^-, TBHP, •OH, and $^1O_2$; 8: 5 μM HOCl; 9–18: 100 μM Mg^{2+}, Cu^{2+}, K^+, Na^+, Fe^{2+}, Ca^{2+}, Zn^{2+}, NO_2^-, NO_3^-, HS^-; 19–20: 1 mM Cl^-, GSH. Partial results are presented as mean ± standard deviation (n = 3).

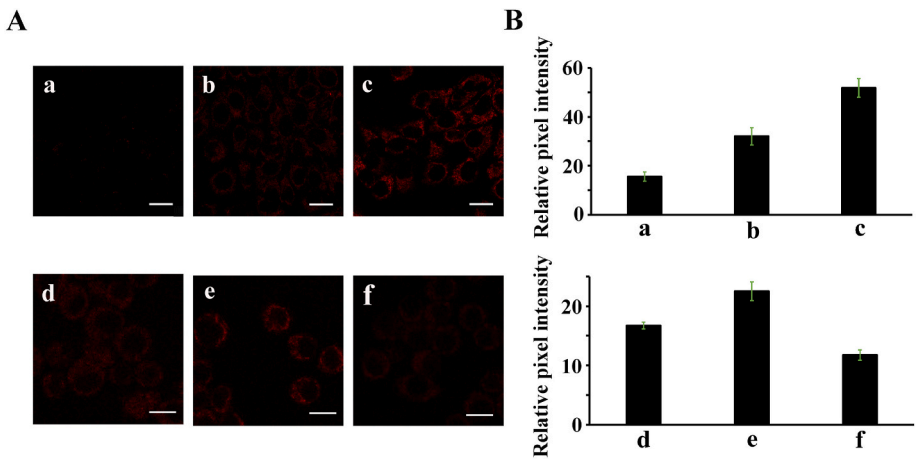

Fig. 6. Confocal experiments in cancer and macrophage cells. (A) Images of the cells. MCF-7 cells incubated with 5 μM **RIC** for 30 min and then treated with (a) 0, (b) 20, and (c) 40 μM HOCl for 30 min, respectively. (d) RAW264.7 cells incubated with 5 μM **RIC** for 30 min. (e) RAW264.7 cells pretreated with LPS (100 ng, 4 h), IFN-γ (30 ng, 4 h), and PMA (10 ng, 30 min) and then incubated with 5 μM **RIC** for 30 min. (f) RAW264.7 cells pretreated with NAC (1 mM, 1 h) and then incubated with 5 μM **RIC** for 30 min. (B) Relative pixel intensity of the related images in (A). The results are presented as mean ± standard deviation (n = 3). Red channels were excited at 543 nm and collected within 553–618 nm. Scale bar: 20 μm. (For interpretation of the references to colour in this figure legend, the reader is referred to the Web version of this article.)

(Fig. S10), showing that **RIC** mainly reacted with OCl^- in buffers. The fluorescence titration experiments showed that I_{580} had a linear relationship with HOCl (Fig. 5C), and the detection limit was calculated to be as low as 3.8 nM (3σ/k, where σ is the standard deviation of the blank fluorescence measurements and k is the slope of the fluorescence intensities over the concentrations of HOCl). Similar to I_{580}, I_{480} also increased and had a linear relationship with HOCl concentrations (Fig. S11), which was probably a result of the structure change.

As shown in Fig. 5D, I_{580} dramatically increased only in the presence of HOCl, indicating the high selectivity of **RIC** toward HOCl. The selectivity ensures that **RIC** is capable of detecting HOCl in complex biological environments containing multiple analytes. In contrast to I_{580}, there was no obvious enhancement of I_{480}, and I_{480} retained most of the intensity upon the addition of biologically relevant analytes (Fig. S12). The relative stability of I_{480} indicated that the inherent blue fluorescence of **RIC** is also not susceptible to fluctuations in analyte concentrations in biological environments, confirming the mitochondria-tracing capacity of **RIC**.

Based on these results, we deduced that **RIC** is able to detect mitochondrial HOCl, which can be ascribed to its mitochondria-anchoring capacity, fast response, high selectivity and sensitivity, and MpH-insensitive detection capability. Hence, we tested whether **RIC** could analyze endogenous and exogenous HOCl in live cells. As depicted in Fig. 6a–c, I_{580} increased with exogenous HOCl concentrations from 0 to

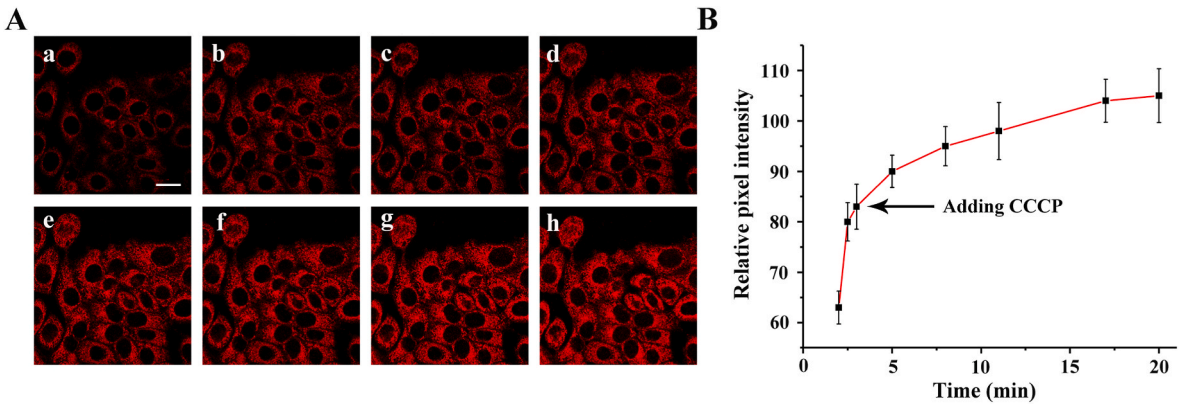

Fig. 7. Confocal experiments in MCF-7 cells. (A) Images of the cells. Cells incubated with 15 μM **RIC** for 30 min and then treated with 50 μM HOCl for (a) 2, (b) 2.5, (c) 3, (d) 5, (e) 8, (f) 11, (g) 17, and (h) 20 min, respectively. During the sensing process, 10 μM CCCP was added at 3 min to quickly depolarize mitochondria. (B) Relative pixel intensity of the related images in (A). The results are presented as mean ± standard deviation (n = 3). Red channels were excited at 543 nm and collected within 553–618 nm. Scale bar: 20 μm. (For interpretation of the references to colour in this figure legend, the reader is referred to the Web version of this article.)

40 μM, indicating that **RIC** semiquantitatively detected exogenous HOCl in cancer cells. Next, we performed endogenous HOCl experiments in RAW264.7 cells. When incubated with **RIC** alone, I_{580} was maintained at a moderate level in the cells (Fig. 6d), and the fluorescence was enhanced when the cells were pretreated with lipopolysaccharide (LPS), interferon gamma (IFN-γ), and phorbol 12-myristate 13-acetate (PMA) to induce cells to produce more HOCl (Fig. 6e) [78], demonstrating that **RIC** is able to sense endogenous HOCl in macrophage cells. As expected, I_{580} was also decreased after another group of cells was pretreated with N-acetylcysteine (NAC) to weaken the native production of HOCl (Fig. 6f) [79], confirming that **RIC** detected endogenous HOCl in macrophage cells. Meanwhile, some of the mitochondria in MCF-7 cells became fragmented after HOCl treatment (Fig. S13), whereas most of the mitochondria in RAW264.7 cells remained in punctate structures (Fig. S14), indicating that the mitochondrial morphology of cancer cells is more susceptible to HOCl than that of macrophages. Photo-stability experiments with **RIC** and HOCl showed negligible changes in I_{480} and I_{580} after 10 rounds of laser scanning (Fig. S15), thus demonstrating the efficient photo-stability of **RIC** under normal test conditions.

Finally, we tested whether the mitochondria-anchoring characteristic of **RIC** facilitated the real-time detection of HOCl in mitochondria. First, colocalization experiments of I_{580} and MTG were performed (Fig. S16). The pictures, scatter plot, and intensity profile indicated that I_{580} was retained in mitochondria after HOCl treatment, and the Pearson's correlation coefficient was calculated as 0.82. Theoretically, the mitochondria-anchoring characteristic of **RIC** and the retention of I_{580} in mitochondria should show that the red fluorescence signal could reflect the fluctuations in mitochondrial HOCl concentrations. To test this hypothesis, we performed real-time HOCl detection experiments in MCF-7 cells.

Excluding the effect of mitochondrial depolarization on the HOCl-sensing performance of **RIC** would have been difficult because HOCl can also depolarize mitochondria. Therefore, we aimed to verify that the alteration of different degrees of MMP caused by the addition of CCCP has a low impact on the real-time HOCl detection. Previous studies indicate that HOCl caused only a negligible reduction of MMP in the first 5 min [81], whereas CCCP caused complete mitochondrial depolarization within 1 min [76,80]. Therefore, we added 10 μM CCCP at 3 min during the sensing application to quickly depolarize mitochondria, which should have induced a marked change of MMP within minutes. We also confirmed the alteration of MMP using TMRM (a commercial dye for MMP). As shown in Fig. S17, the red fluorescence of TMRM faded in the presence of CCCP, confirming a marked change of MMP after the addition of CCCP at 3 min. When HOCl was added to the cells, I_{580} increased sharply at the beginning and then gradually, as shown in Fig. 7, which was in agreement with the cellular HOCl uptake rates reported in a previous study [81]. In contrast to marked change in MMP, the dynamic fluorescence intensity curve of I_{580} was not altered much upon the addition of CCCP, for example, the slopes between 2.5, 3, and 5 min showed that MMP had a low impact on the real-time detection of HOCl. Meanwhile, when mitochondrial depolarization happened in the presence of both HOCl and CCCP, a serious dye leakage should have occurred and the intensity curve should have stopped increasing immediately due to the fast response of **RIC** toward HOCl, if **RIC** did not have the mitochondria-anchoring property. Therefore, these results suggest that the mitochondria-anchoring characteristic of **RIC** facilitates the real-time detection of mitochondrial HOCl in live cells.

4. Conclusions

Considering the current lack and real significance of mitochondria-tracing HOCl probes, we designed and synthesized three dyes and selected **RIC** for real-time detection of mitochondrial dynamics and HOCl in live cells. Owing to its mitochondria-anchoring capability and steady inherent fluorescence signal, **RIC** traced both polarized and depolarized mitochondria and real-time detected CCCP-induced morphological changes of mitochondria in MCF-7 cells. In addition, the fast response, high selectivity and sensitivity, and MpH-insensitive detection of HOCl enabled **RIC** to real-time detect endogenous and exogenous HOCl in mitochondria. All the sensing characteristics presented in this article suggest that **RIC** is a powerful tool for potential research in biology involving both mitochondrial dynamics and HOCl. The molecular design strategy also offers a general method for synthesizing new multifunctional probes for mitochondrial HOCl.

CRediT authorship contribution statement

Nansong Zhu: Methodology, Validation, Formal analysis, conducted the experiments, analyzed experimental results, Writing – original draft. **Xiaolei Guo:** Formal analysis. **Yulei Chang:** Assisted in preparation of the molecules, Funding acquisition, Writing – review & editing. **Zhan Shi:** Conceptualization, Methodology, Investigation, Resources, Supervision, Project administration, Funding acquisition, Writing – review & editing. **Long Yi Jin:** Supervision, Funding acquisition, Writing – review & editing. **Shouhua Feng:** Writing – review & editing.

Declaration of competing interest

The authors declare that they have no known competing financial interests or personal relationships that could have appeared to influence

the work reported in this paper.

Acknowledgements

This work was financially supported by the National Natural Science Foundation of China (21961041, 21771077, 21771084, 62075217), and the Foundation of Science and Technology Development of Jilin Province, China (20200801004GH).

Appendix A. Supplementary data

Supplementary data to this article can be found online at https://doi.org/10.1016/j.dyepig.2022.110227.

References

[1] Du EJ, Ahn TJ, Kwon I, Lee JH, Park JH, Park SH, et al. TrpA1 regulates defecation of food-borne pathogens under the control of the duox pathway. PLoS Genet 2016;12(1):e1005773.
[2] Winterbourn CC, Kettle AJ, Hampton MB. Reactive oxygen species and neutrophil function. Annu Rev Biochem 2016;85(1):765–92.
[3] Aratani Y. Myeloperoxidase: its role for host defense, inflammation, and neutrophil function. Arch Biochem Biophys 2018;640:47–52.
[4] Wu D, Chen L, Xu Q, Chen X, Yoon J. Design principles, sensing mechanisms, and applications of highly specific fluorescent probes for HOCl/OCl^-. Acc Chem Res 2019;52(8):2158–68.
[5] Wu L, Sedgwick AC, Sun X, Bull SD, He XP, James TD. Reaction-based fluorescent probes for the detection and imaging of reactive oxygen, nitrogen, and sulfur species. Acc Chem Res 2019;52(9):2582–97.
[6] Duan C, Won M, Verwilst P, Xu J, Kim HS, Zeng L, et al. In vivo imaging of endogenously produced HClO in zebrafish and mice using a bright, photostable ratiometric fluorescent probe. Anal Chem 2019;91(6):4172–8.
[7] Zhang B, Yang X, Zhang R, Liu Y, Ren X, Xian M, et al. Lysosomal-targeted two-photon fluorescent probe to sense hypochlorous acid in live cells. Anal Chem 2017;89(19):10384–90.
[8] Yue Y, Huo F, Yin C, Escobedo JO, Strongin RM. Recent progress in chromogenic and fluorogenic chemosensors for hypochlorous acid. Analyst 2016;141(6):1859–73.
[9] Pak YL, Park SJ, Wu D, Cheon B, Kim HM, Bouffard J, et al. N-Heterocyclic carbene boranes as reactive oxygen species-responsive materials: application to the two-photon imaging of hypochlorous acid in living cells and tissues. Angew Chem Int Ed 2018;57(6):1567–71.
[10] Winterbourn CC. The challenges of using fluorescent probes to detect and quantify specific reactive oxygen species in living cells. Biochim Biophys Acta 2014;1840(2):730–8.
[11] Dou K, Fu Q, Chen G, Yu F, Liu Y, Cao Z, et al. A novel dual-ratiometric-response fluorescent probe for SO_2/ClO^- detection in cells and in vivo and its application in exploring the dichotomous role of SO_2 under the ClO^- induced oxidative stress. Biomaterials 2017;133:82–93.
[12] Zhang P, Wang H, Hong Y, Yu M, Zeng R, Long Y, et al. Selective visualization of endogenous hypochlorous acid in zebrafish during lipopolysaccharide-induced acute liver injury using a polymer micelles-based ratiometric fluorescent probe. Biosens Bioelectron 2018;99:318–24.
[13] Xie X, Wu T, Wang X, Li Y, Wang K, Zhao Z, et al. A two-photon fluorescent probe for ratiometric visualization of hypochlorous acid in live cells and animals based on a selenide oxidation/elimination tandem reaction. Chem Commun 2018;54(84):11965–8.
[14] Chen X, Wang F, Hyun JY, Wei T, Qiang J, Ren X, et al. Recent progress in the development of fluorescent, luminescent and colorimetric probes for detection of reactive oxygen and nitrogen species. Chem Soc Rev 2016;45(10):2976–3016.
[15] Kwon N, Kim D, Swamy KMK, Yoon J. Metal-coordinated fluorescent and luminescent probes for reactive oxygen species (ROS) and reactive nitrogen species (RNS). Coord Chem Rev 2021;427:213581–606.
[16] He L, Zhang Y, Xiong H, Wang J, Geng Y, Wang B, et al. A ratiometric flavone-based fluorescent probe for hypochlorous acid detection with large Stokes shift and long-wavelength emission. Dyes Pigments 2019;166:390–4.
[17] Koide Y, Urano Y, Hanaoka K, Terai T, Nagano T. Development of an Si-rhodamine-based far-red to near-infrared fluorescence probe selective for hypochlorous acid and its applications for biological imaging. J Am Chem Soc 2011;133(15):5680–2.
[18] Xu Q, Lee KA, Lee S, Lee KM, Lee WJ, Yoon J. A highly specific fluorescent probe for hypochlorous acid and its application in imaging microbe-induced HOCl production. J Am Chem Soc 2013;135(26):9944–9.
[19] Zhang Q, Zhu Z, Zheng Y, Cheng J, Zhang N, Long YT, et al. A three-channel fluorescent probe that distinguishes peroxynitrite from hypochlorite. J Am Chem Soc 2012;134(45):18479–82.
[20] Zhang R, Zhao J, Han G, Liu Z, Liu C, Zhang C, et al. Real-Time discrimination and versatile profiling of spontaneous reactive oxygen species in living organisms with a single fluorescent probe. J Am Chem Soc 2016;138(11):3769–78.
[21] Zhu H, Fan J, Wang J, Mu H, Peng X. An "enhanced PET"-based fluorescent probe with ultrasensitivity for imaging basal and elesclomol-induced HClO in cancer cells. J Am Chem Soc 2014;136(37):12820–3.
[22] Chan J, Dodani SC, Chang CJ. Reaction-based small-molecule fluorescent probes for chemoselective bioimaging. Nat Chem 2012;4(12):973–84.
[23] Hu JJ, Wong N-K, Gu Q, Bai X, Ye S, Yang D. HKOCl-2 series of green BODIPY-based fluorescent probes for hypochlorous acid detection and imaging in live cells. Org Lett 2014;16(13):3544–7.
[24] Zhang Y-R, Liu Y, Feng X, Zhao B-X. Recent progress in the development of fluorescent probes for the detection of hypochlorous acid. Sens Actuators, B 2017;240:18–36.
[25] Gan Y, Yin G, Zhang X, Zhou L, Zhang Y, Li H, et al. Turn-on fluorescent probe for sensing exogenous and endogenous hypochlorous acid in living cells, zebrafishes and mice. Talanta 2021;225:122030–7.
[26] Zhang R, Song B, Yuan J. Bioanalytical methods for hypochlorous acid detection: recent advances and challenges. TrAC Trends Anal Chem (Reference Ed) 2018;99:1–33.
[27] Ma C, Zhong G, Zhao Y, Zhang P, Fu Y, Shen B. Recent development of synthetic probes for detection of hypochlorous acid/hypochlorite. Spectrochim Acta, Part A 2020;240:118545–57.
[28] Świerczyńska M, Słowiński D, Grzelakowska A, Szala M, Romański J, Pierzchała K, et al. Selective, stoichiometric and fast-response fluorescent probe based on 7-nitrobenz-2-oxa-1,3-diazole fluorophore for hypochlorous acid detection. Dyes Pigments 2021;193:109563–72.
[29] Yue X, Wang J, Han J, Wang B, Song X. A dual-ratiometric fluorescent probe for individual and continuous detection of H_2S and HClO in living cells. Chem Commun 2020;56(19):2849–52.
[30] Zhang W, Wang H, Li F, Chen Y, Kwok RTK, Huang Y, et al. A ratiometric fluorescent probe based on AIEgen for detecting HClO in living cells. Chem Commun 2020;56(93):14613–6.
[31] Wang S, Zhu B, Wang B, Cao X, Zhu L, Hou J-T, et al. Revealing HOCl burst from endoplasmic reticulum in cisplatin-treated cells via a ratiometric fluorescent probe. Chin Chem Lett 2021;32(5):1795–8.
[32] He X, Deng Z, Xu W, Li Y, Xu C, Chen H, et al. A novel dual-response chemosensor for bioimaging of Exogenous/Endogenous hypochlorite and hydrazine in living cells, Pseudomonas aeruginosa and zebrafish. Sens Actuators, B 2020;321:128450–60.
[33] Qian X, Yu H, Zhu W, Yao X, Liu W, Yang S, et al. Near infrared fluorescent probe for in vivo bioimaging of endogenous hypochlorous acid. Dyes Pigments 2021;188:109218–23.
[34] Xiao H, Xin K, Dou H, Yin G, Quan Y, Wang R. A fast-responsive mitochondria-targeted fluorescent probe detecting endogenous hypochlorite in living RAW 264.7 cells and nude mouse. Chem Commun 2015;51(8):1442–5.
[35] Gao P, Pan W, Li N, Tang B. Fluorescent probes for organelle-targeted bioactive species imaging. Chem Sci 2019;10(24):6035–71.
[36] Zhou J, Li L, Shi W, Gao X, Li X, Ma H. HOCl can appear in the mitochondria of macrophages during bacterial infection as revealed by a sensitive mitochondrial-targeting fluorescent probe. Chem Sci 2015;6(8):4884–8.
[37] Chen Y, Wei T, Zhang Z, Zhang W, Lv J, Chen T, et al. A mitochondria-targeted fluorescent probe for ratiometric detection of hypochlorite in living cells. Chin Chem Lett 2017;28(10):1957–60.
[38] Yuan L, Wang L, Agrawalla BK, Park SJ, Zhu H, Sivaraman B, et al. Development of targetable two-photon fluorescent probes to image hypochlorous acid in mitochondria and lysosome in live cell and inflamed mouse model. J Am Chem Soc 2015;137(18):5930–8.
[39] Ren M, Zhou K, He L, Lin W. Mitochondria and lysosome-targetable fluorescent probes for HOCl: recent advances and perspectives. J Mater Chem B 2018;6(12):1716–33.
[40] Jiao X, Huang K, He S, Liu C, Zhao L, Zeng X. A mitochondria-targeted near-infrared fluorescent probe with a large Stokes shift for real-time detection of hypochlorous acid. Org Biomol Chem 2018;17(1):108–14.
[41] Zheng A, Liu H, Peng C, Gao X, Xu K, Tang B. A mitochondria-targeting near-infrared fluorescent probe for imaging hypochlorous acid in cells. Talanta 2021;226:122152–8.
[42] Hou JT, Wu MY, Li K, Yang J, Yu KK, Xie YM, et al. Mitochondria-targeted colorimetric and fluorescent probes for hypochlorite and their applications for in vivo imaging. Chem Commun 2014;50(63):8640–3.
[43] Zhu B, Wu L, Zhang M, Wang Y, Liu C, Wang Z, et al. A highly specific and ultrasensitive near-infrared fluorescent probe for imaging basal hypochlorite in the mitochondria of living cells. Biosens Bioelectron 2018;107:218–23.
[44] Xu J, Wang C, Ma Q, Zhang H, Tian M, Sun J, et al. Novel mitochondria-targeting and naphthalimide-based fluorescent probe for detecting HClO in living cells. ACS Omega 2021;6(22):14399–409.
[45] Wang B, Yuan F, Wang S, Duan R, Ren WX, Hou J-T. Detection of atherosclerosis-associated HOCl using a mitochondria-targeted fluorescent probe. Sens Actuators, B 2021;348:130695–703.
[46] Gao Y, Sun R, Zhao M, Ding J, Wang A, Ye S, et al. Sulfenic acid-mediated on-site-specific immobilization of mitochondrial-targeted NIR fluorescent probe for prolonged tumor imaging. Anal Chem 2020;92(10):6977–83.
[47] Holmila RJ, Vance SA, Chen X, Wu H, Shukla K, Bharadwaj MS, et al. Mitochondria-targeted probes for imaging protein sulfenylation. Sci Rep 2018;8(1):6635–48.
[48] Lee MH, Park N, Yi C, Han JH, Hong JH, Kim KP, et al. Mitochondria-immobilized pH-sensitive off-on fluorescent probe. J Am Chem Soc 2014;136(40):14136–42.
[49] Li MY, Li K, Liu YH, Zhang H, Yu KK, Liu X, et al. Mitochondria-immobilized fluorescent probe for the detection of hypochlorite in living cells, tissues, and zebrafishes. Anal Chem 2020;92(4):3262–9.

[50] Li X, Hu Y, Li X, Ma H. Mitochondria-immobilized near-infrared ratiometric fluorescent pH probe to evaluate cellular mitophagy. Anal Chem 2019;91(17):11409–16.
[51] Wang B, Zhang X, Wang C, Chen L, Xiao Y, Pang Y. Bipolar and fixable probe targeting mitochondria to trace local depolarization via two-photon fluorescence lifetime imaging. Analyst 2015;140(16):5488–94.
[52] Zhang X, Sun Q, Huang Z, Huang L, Xiao Y. Immobilizable fluorescent probes for monitoring the mitochondria microenvironment: a next step from the classic. J Mater Chem B 2019;7(17):2749–58.
[53] Zhang R, Niu G, Li X, Guo L, Zhang H, Yang R, et al. Reaction-free and MMP-independent fluorescent probes for long-term mitochondria visualization and tracking. Chem Sci 2019;10(7):1994–2000.
[54] Murale DP, Haque MM, Hong SC, Jang S-y, Lee JH, An SJ, et al. Development of a bifunctional BODIPY probe for mitochondria imaging and in situ photo-crosslinking in live cell. Dyes Pigments 2021;196:109830–9.
[55] Wang X, Chen Q, Ou J, Huang Y, Wang C, Chen Y-a, et al. Real-time and accurate monitoring of mitochondria-related apoptosis by a multifunctional two-photon fluorescent probe. Sens Actuators, B 2022;351:130953–9.
[56] Zhu N, Guo X, Pang S, Chang Y, Liu X, Shi Z, et al. Mitochondria-immobilized unimolecular fluorescent probe for multiplexing imaging of living cancer cells. Anal Chem 2020;92(16):11103–10.
[57] Kaewsuya P, Danielson ND, Ekhterae D. Fluorescent determination of cardiolipin using 10-N-nonyl acridine orange. Anal Bioanal Chem 2007;387(8):2775–82.
[58] Liang Z, Sun Y, Duan R, Yang R, Qu L, Zhang K, et al. Low polarity-triggered basic hydrolysis of coumarin as an AND logic gate for broad-spectrum cancer diagnosis. Anal Chem 2021;93(36):12434–40.
[59] Tilokani L, Nagashima S, Paupe V, Prudent J. Mitochondrial dynamics: overview of molecular mechanisms. Essays Biochem 2018;62(3):341–60.
[60] Wang JL, Zhang L, Gao LX, Chen JL, Zhou T, Liu Y, et al. A bright, red-emitting water-soluble BODIPY fluorophore as an alternative to the commercial Mito Tracker Red for high-resolution mitochondrial imaging. J Mater Chem B 2021;9(41):8639–45.
[61] Ni HM, Williams JA, Ding WX. Mitochondrial dynamics and mitochondrial quality control. Redox Biol 2015;4:6–13.
[62] Li X, Long C, Cui Y, Tao F, Yu X, Lin W. Charge-dependent strategy enables a single fluorescent probe to study the interaction relationship between mitochondria and lipid droplets. ACS Sens 2021;6(4):1595–603.
[63] Guo L, Liu H, Jin X, Zhang Z, Su J, Yu X. Development of reaction-free and mitochondrion-immobilized fluorescent probe for monitoring pH change. Sens Actuators, B 2021;341:129962–70.
[64] Rodriguez-Enriquez S, Kim I, Currin RT, Lemasters JJ. Tracker dyes to probe mitochondrial autophagy (mitophagy) in rat hepatocytes. Autophagy 2006;2(1):39–46.
[65] Hou JT, Li K, Yang J, Yu KK, Liao YX, Ran YZ, et al. A ratiometric fluorescent probe for in situ quantification of basal mitochondrial hypochlorite in cancer cells. Chem Commun 2015;51(31):6781–4.
[66] Ji W, Tang X, Du W, Lu Y, Wang N, Wu Q, et al. Optical/electrochemical methods for detecting mitochondrial energy metabolism. Chem Soc Rev 2022;51(1):71–127.
[67] Jiang C, Huang H, Kang X, Yang L, Xi Z, Sun H, et al. NBD-based synthetic probes for sensing small molecules and proteins: design, sensing mechanisms and biological applications. Chem Soc Rev 2021;50(13):7436–95.
[68] Wang Y-B, Luo H-Z, Wang C-Y, Guo Z-Q, Zhu W-H. A turn-on fluorescent probe based on π-extended coumarin for imaging endogenous hydrogen peroxide in RAW 264.7 cells. J Photochem Photobiol, A 2021;414:113270–6.
[69] Yang X, Jin L, Chen Y, Zhong X, Jiang Y, Dai Z. A novel aggregation induced emission probe based on coumarin scaffold for imaging hypochlorite in cells and zebrafish. J Photochem Photobiol, A 2021;419:113464–71.
[70] Yuan L, Lin W, Cao Z, Wang J, Chen B. Development of FRET-based dual-excitation ratiometric fluorescent pH probes and their photocaged derivatives. Chem Eur J 2012;18(4):1247–55.
[71] Wang Z, Hao C, Luo X, Wu Q, Zhang C, Dessie W, et al. A FRET-ICT dual-modulated ratiometric fluorescence sensor for monitoring and bio-imaging of cellular selenocysteine. Molecules 2020;25(21):4999–5011.
[72] Liu Z, Wang Q, Wang H, Su W, Dong S. A FRET based two-photon fluorescent probe for visualizing mitochondrial thiols of living cells and tissues. Sensors 2020;20(6):1746–57.
[73] Grimm JB, English BP, Chen J, Slaughter JP, Zhang Z, Revyakin A, et al. A general method to improve fluorophores for live-cell and single-molecule microscopy. Nat Methods 2015;12(3):244–50.
[74] Naganbabu M, Perkins LA, Wang Y, Kurish J, Schmidt BF, Bruchez MP. Multiexcitation fluorogenic labeling of surface, intracellular, and total protein pools in living cells. Bioconjugate Chem 2016;27(6):1525–31.
[75] Agnello M, Morici G, Rinaldi AM. A method for measuring mitochondrial mass and activity. Cytotechnology 2008;56(3):145–9.
[76] Perry SW, Norman JP, Barbieri J, Brown EB, Gelbard HA. Mitochondrial membrane potential probes and the proton gradient: a practical usage guide. Biotechniques 2011;50(2):98–115.
[77] Bantseev V. Optical function and mitochondrial metabolic properties in damage and recovery of bovine lens after in vitro carbonyl cyanide m-chlorophenylhydrazone treatment. Mitochondrion 2003;3(1):1–11.
[78] Xu Q, Heo CH, Kim JA, Lee HS, Hu Y, Kim D, et al. A selective imidazoline-2-thione-bearing two-photon fluorescent probe for hypochlorous acid in mitochondria. Anal Chem 2016;88(12):6615–20.
[79] Selloum L, Djelili H, Sebihi L, Arnhold J. Scavenger effect of flavonols on HOCl-induced luminol chemiluminescence. Luminescence 2004;19(4):199–204.
[80] Nieminen AL, Saylor AK, Tesfai SA, Herman B, Lemasters JJ. Contribution of the mitochondrial permeability transition to lethal injury after exposure of hepatocytes to *t*-butylhydroperoxide. Biochem J 1995;307:99–106.
[81] Whiteman M, Rose P, Siau JL, Cheung NS, Tan GS, Halliwell B, et al. Hypochlorous acid-mediated mitochondrial dysfunction and apoptosis in human hepatoma HepG2 and human fetal liver cells: role of mitochondrial permeability transition. Free Radical Biol Med 2005;38(12):1571–84.